Continuous-time quantum walks on a defective lattice: boosting the spreading of delocalized states through Parrondo's strategy

João V. Cordeiro, Eduardo I. Duzzioni, and Edgard P. M. Amorim^{1,*}

We investigate the quantum transport of delocalized states in continuous-time quantum walks (CTQWs) on a one-dimensional lattice containing a single defect. The defect is modeled by assigning complex-valued hopping amplitudes to the edges that connect the site corresponding to the mean position of the initial delocalized state to its nearest neighbors. We find that this single defective site is sufficient to enhance the ballistic spreading of an initially Gaussian wave packet. Extending these results, we implement a time-dependent alternation protocol between two distinct defect configurations, each individually yielding poor propagation of the state. The combination of these two unfavorable configurations improves the transport efficiency of the quantum walker, revealing a manifestation of Parrondo's paradox in CTQWs with delocalized initial states. This study provides new insights into the role of complex-phase defects and time-dependent protocols in CTQWs, demonstrating that the interplay between quantum interference and graph engineering can effectively enhance quantum transport in discrete lattices.

I. INTRODUCTION

Quantum walks (QWs), the quantum analogs of classical random walks, have emerged as fundamental models in quantum information processing and quantum computing, providing a universal platform for the development of quantum algorithms. The concept was initially proposed in 1993 by Aharonov et al. in a discrete-time formulation [1] and later extended to a continuous-time framework in 1998 by Farhi and Gutmann [2]. These models exhibit unique features compared to classical random walks, such as quantum interference and ballistic transport [3, 4], making them key tools for exploring quantum phenomena and their applications. The ballistic propagation of quantum walks motivated their early applications as quantum search engines [5–7], yet they have since been employed to model a wide range of physical processes, including photosynthesis [8, 9] and universal computation [10, 11]. Furthermore, quantum walks have been implemented across diverse experimental settings [12, 13].

The transport properties of quantum walks are sensitive to both dynamical and spatial variations [14–23]. When quantum coins are chosen randomly over time, the walker exhibits diffusive behavior [14], whereas spatial disorder along the lattice leads to Anderson localization [15]. Even a single lattice defect may be sufficient to trap or localize the quantum state [16–21], although in some cases it may also enhance its propagation [22, 23]. Since the algorithmic efficiency of quantum walks depends on improving their ballistic spreading, strategies that promote faster walker propagation can be regarded as successful, in contrast to those that localize or trap the state [24].

In this context, an intriguing link arises between game theory and quantum mechanics through Parrondo's effect in quantum phenomena [25]. Parrondo's effect describes apparently paradoxical situations in which losing strategies or adverse effects combine to produce a winning outcome [26, 27]. This effect has been explored across several fields. For instance, it has been used to explain complex adaptations in biological systems [28, 29], to optimize crop rotations in agriculture [30], to analyze complex networks [31], and to design routing strategies [32]. Turning to quantum walks, one may wonder whether alternating over time between two individual lattice defects, each leading to poor spreading, would also result in a weak outcome. This question was recently addressed by Ximenes et al. [23]. In their study, the authors modified the hopping amplitudes at a single site and identified two distinct hopping configurations, each of which individually leads to poor spreading. They then demonstrated the Parrondo's effect, showing that alternating between these two configurations during the walk enhances the walker's propagation, thereby outperforming the case without hopping modulation.

Although several studies have investigated Parrondo's effect in discrete-time quantum walks [33–41], to the best of our knowledge, Ximenes et al. were the first to demonstrate this effect in CTQWs [23]. Their analysis, however, was restricted to a single localized initial state and real hopping amplitudes. By relaxing the condition of a localized initial state and instead considering a superposition of position states, one can also explore the phase effects introduced by complex hopping amplitudes in such systems. Indeed, several studies have revealed novel features of quantum walks starting from delocalized initial conditions [42–47], such as the emergence of soliton-like behavior [49], which could enable high-fidelity state transfer protocols [50, 51]. Other studies have demonstrated chiral control of quantum information driven by such complex hopping amplitudes [52–54].

¹Departamento de Física, Universidade do Estado de Santa Catarina, 89219-710, Joinville, SC, Brazil ²Departamento de Física, Universidade Federal de Santa Catarina, 88040-900, Florianópolis, SC, Brazil (Dated: November 13, 2025)

^{*} edgard.amorim@udesc.br

In the present study, we investigate the dynamics of a one-dimensional CTQW on a defective lattice starting from a Gaussian state, employing a Parrondo-based strategy to enhance the spreading of the walker. The defect is introduced through complex hopping amplitudes between the site corresponding to the mean position of the initial Gaussian state and its nearest neighbors. We systematically explore the influence of both the real and imaginary components of the hopping amplitude, thereby identifying regions associated with good or poor spreading regimes relative to the defect-free case. Subsequently, we implement Parrondo's strategy, showing a significant enhancement in the spreading of the delocalized state.

This article is organized as follows. Section II presents the mathematical formalism of the CTQW model on a defective lattice, considering a Gaussian distribution as the initial state. Section III discusses the spreading behavior of the delocalized state under complex defects and the implementation of Parrondo's strategy. Finally, Section IV summarizes the main conclusions.

II. MATHEMATICAL FORMALISM

The following subsections present the theoretical framework of CTQWs, describing how a defect is incorporated into the one-dimensional lattice, the delocalized initial state considered here, and the alternation protocol employed to implement Parrondo's strategy.

A. Continuous-time quantum walks

The CTQW model explored here describes the motion of a quantum particle on an infinite line composed of discrete sites. The quantum particle can hop only between neighboring sites, i.e., from the site j to $j\pm 1$. A quantum state $|\psi\rangle$ associated with the particle evolves by the time-dependent Schrödinger equation,

$$i\hbar \frac{\partial}{\partial t} |\psi(t)\rangle = \hat{H} |\psi(t)\rangle,$$
 (1)

with the Hamiltonian for a CTQW on a homogeneous lattice given by

$$\hat{H} = \epsilon \sum_{j} |j\rangle \langle j| - \gamma \sum_{j} (|j-1\rangle \langle j| + |j+1\rangle \langle j|), \quad (2)$$

where ϵ denotes the constant on-site potential energy and γ the hopping amplitude between neighboring sites.

After obtaining $|\psi(t)\rangle$, the probability of finding the particle at site j is

$$P_j(t) = \left| \langle j | \psi(t) \rangle \right|^2, \tag{3}$$

and to quantify the spreading of the particle, we consider the standard deviation,

$$\sigma(t) = \sqrt{\langle j^2 \rangle - \langle j \rangle^2},\tag{4}$$

where $\langle j^n \rangle = \langle \psi(t) | j^n | \psi(t) \rangle$ denotes the *n*-th moment of the position distribution. Since the quantum walker exhibits ballistic behavior, its variance grows quadratically faster than in the classical diffusive case, leading to $\sigma \propto t$ instead of $\sigma \propto \sqrt{t}$. For $t \gg 1$, the quantum walker reaches the long-time regime [47], where the slope or the time derivative of the standard deviation,

$$\alpha = \frac{d\sigma(t)}{dt},\tag{5}$$

quantifies the walker's long-time spreading rate.

B. CTQW on the defective lattice

Previous studies have investigated the transport of a quantum particle in one-dimensional CTQWs on lattices containing a single defect [22, 23]. Such a defect can be modeled by modifying the hopping amplitudes between a specific site j=d and its neighboring sites $d\pm 1$. We therefore consider the following Hamiltonian

$$\hat{H}_d = \hat{H} + \gamma (\hat{V}_d + \hat{V}_d^{\dagger}), \tag{6}$$

where \hat{V}_d^{\dagger} is the Hermitian conjugate of \hat{V}_d , and the defect operator is defined as

$$\hat{V}_d = (1 - \xi e^{i\theta_-}) |d - 1\rangle \langle d| + (1 - \xi e^{i\theta_+}) |d + 1\rangle \langle d|.$$
 (7)

This formulation implies that the hoppings from site d to its nearest neighbors $d\pm 1$ are scaled by dimensionless complex factors $\xi e^{i\theta\pm}$, while the reverse hoppings from sites $d\pm 1$ to d are multiplied by their corresponding complex conjugates. For $\theta_-\neq\theta_+$, the model introduces distinct phases in the left and right hopping amplitudes. Finally, the Hamiltonian \hat{H}_d reduces to \hat{H} when $\xi=1$ and $\theta_-=\theta_+$, whereas $\xi=0$ completely decouples site d, trapping the probability amplitude of the quantum walker at that position. Figure 1 illustrates the defective lattice model.

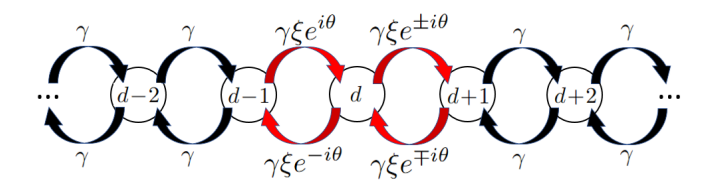


FIG. 1. Schematic representation of a CTQW on a defective lattice. The hopping amplitudes from site d to its nearest neighbors $d\pm 1$ are multiplied by $\xi e^{i\theta\pm}$, whereas all other hopping amplitudes are real and equal to γ . Two scenarios are considered: (i) both phases are equal, $\theta_-=\theta_+=\theta$, and (ii) the phases have opposite signs, $\theta_-=\theta$ and $\theta_+=-\theta$. Throughout this study from here, we assume $\epsilon=0$ from \hat{H} in Eq. (6) and take d=0 for convenience.

C. Delocalized initial state

In this work, we consider an initial quantum state represented as a superposition of site basis states,

$$|\psi_0\rangle = \sum_j \psi(j) |j\rangle,$$
 (8)

where $\psi(j)$ is a distribution function constrained by the normalization condition $\sum_{j} |\psi(j)|^2 = 1$. Instead of the delta function $\psi(j) = \delta_{j,0}$ which represents a localized state in previous studies [22, 23], we consider a Gaussian distribution,

$$\psi(j) = Ae^{-\frac{j^2}{4\sigma_0^2}},\tag{9}$$

where $|\psi(j)|^2$ represents a Gaussian profile centered at the origin, and σ_0 denotes the initial standard deviation of the distribution. For sufficiently delocalized states $(\sigma_0 \geq 1)$, the normalization constant A is well approximated by $(2\pi\sigma_0^2)^{-1/4}$.

It is worth emphasizing that complex-weighted hopping amplitudes play a significant role in the transport properties of delocalized states by inducing chiral propagation, as shown in earlier works [52–54] and further discussed in Section III.

D. Parrondo protocol

The protocol implements the quantum analogue of Parrondo's paradox by alternating the system dynamics between two distinct defective configurations, each corresponding to a poor-spreading regime. In this protocol, we consider two Hamiltonians, \hat{H}_d^A and \hat{H}_d^B , obtained from Eq. (6) using two different parameter sets:

$$(\xi^A, \theta_+^A, \theta_-^A)$$
 and $(\xi^B, \theta_+^B, \theta_-^B)$. (10)

Each half-cycle of the protocol evolves the system under one of the Hamiltonians, \hat{H}_d^A or \hat{H}_d^B , for a fixed time interval π/ω , thereby defining the time-dependent Hamiltonian:

$$\hat{H}_{AB}(t) = \begin{cases} \hat{H}_d^A, & 0 \le t < \pi/\omega, \\ \hat{H}_d^B, & \pi/\omega \le t < 2\pi/\omega, \end{cases}$$
(11)

where ω is the angular frequency corresponding to a full cycle of period $T=2\pi/\omega$, then $\hat{H}_{AB}(t+T)=\hat{H}_{AB}(t)$. The dynamics proceeds as follows. The initial quantum state first evolves under \hat{H}_d^A , after which the resulting state evolves under \hat{H}_d^B . This sequence is then repeated, and the successive alternations determine the long-time spreading behavior of the walker.

III. RESULTS AND DISCUSSION

The following subsections present the main results and discuss their implications. We begin by analyzing the spreading of a continuous Gaussian state, which serves as a reference for comparison with our discrete-lattice simulations. Next, we examine how a CTQW on a defective lattice initiated from a Gaussian state behaves relative to the localized case. Finally, we map the parameter space to identify three specific configurations in which the state exhibits enhanced propagation through Parrondo's strategy.

A. Spreading of a Gaussian state

Although the evolution in CTQWs involves solving the Schrödinger equation using a discrete Laplacian operator [55], it is convenient to examine the continuous case for comparison with the numerical results. Consider a one-dimensional free-particle wave packet given by the distribution function $\phi(x) = Ae^{-x^2/4\sigma_0^2}$, i.e., a continuous-position version of Eq. (9). For convenience, we set $\gamma = 1/(2m)$ and $\hbar = 1$ in the Schrödinger equation. The Hamiltonian becomes

$$\hat{H} = -\gamma \frac{\partial^2}{\partial x^2},\tag{12}$$

then, the evolved state is given by

$$|\phi(t)\rangle = e^{-i\hat{H}t} |\phi(0)\rangle.$$
 (13)

The evolution of a free Gaussian wave packet can be found in many quantum mechanics textbooks [56–58]. After some algebraic manipulation, the standard deviation gives

$$\sigma(t) = \sqrt{\sigma_0^2 + \gamma^2 \frac{t^2}{\sigma_0^2}},\tag{14}$$

which results for $t \gg 1$ in an asymptotic spreading rate

$$\alpha_a \approx \gamma/\sigma_0.$$
 (15)

Therefore, although a Gaussian wave packet spreads ballistically, the rate at which it happens drops as the initial width of the wave packet increases.

It is straightforward to see that as $\sigma_0 \to 0$, neither $\psi(j)$ nor $\phi(x)$ provides an appropriate normalization of the state within the interval $0 < \sigma_0 < 1$. In such cases, both wave functions demand a renormalization of the state by using an Error function $\operatorname{Erf}(z) = (2/\sqrt{\pi}) \int_0^z e^{-u^2} du$ [46]. It implies that the corrected function to express the asymptotic spreading rate from a Gaussian state, in the limit $\sigma_0 \to 0$, is

$$\alpha_c \approx \frac{\gamma}{\sigma_0} \text{Erf}\left(\sqrt{\frac{\pi}{2}}\sigma_0\right).$$
 (16)

Notice this expression connects the spreading rate of the Gaussian-state standard deviation to the value $\alpha = \sqrt{2}$ corresponding to a localized state $|\psi_0\rangle = |0\rangle$. Figure 2 compares spreading rates from CTQWs calculations with expressions α_c and α_a above.

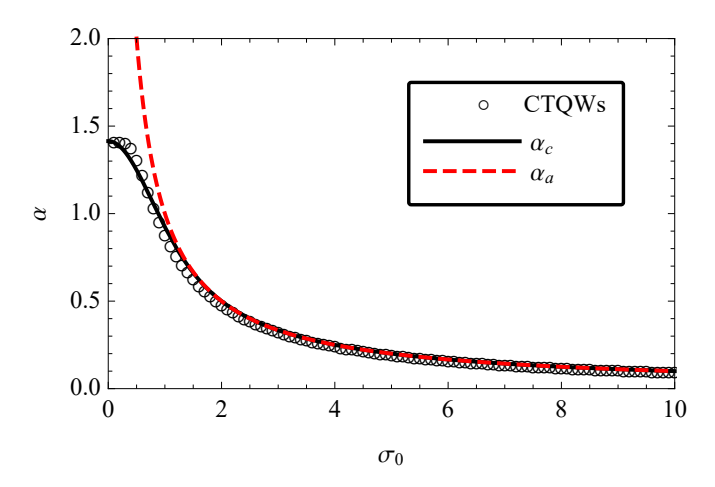


FIG. 2. Spreading rates α of the standard deviation versus σ_0 obtained for CTQWs evolved up to $\gamma t = 1000$ (black empty circle) from Gaussian initial states. The analytical expression α_c is the corrected spreading rate using the Error function given by Eq. (16) (black line), and α_a is the asymptotic spreading rate from Eq. (15) (red dashed line). Both expressions take $\gamma = 1$.

B. Gaussian states on the defective lattice

In the previous section, we analyzed the long-time spreading dynamics of Gaussian wave packets, governed by the Schrödinger equation as a function of their standard deviation σ_0 . Although the evolution remains ballistic, the spreading rate α decreases asymptotically as σ_0 increases. In contrast to a delta-localized state, whose momentum-space representation is uniform, a Gaussian state exhibits a Gaussian momentum distribution. As σ_0 increases, this distribution narrows, suppressing highmomentum components and thereby reducing the effective spreading rate. This behavior directly reflects the Heisenberg uncertainty principle: a larger initial spatial width implies a smaller momentum spread, limiting the contribution of fast-propagating components to the wave-packet evolution.

From an experimental perspective, perfectly localized states are unattainable. Any realistic wave packet necessarily exhibits finite spatial and momentum uncertainties arising from intrinsic quantum limits and extrinsic classical imperfections introduced during state preparation. Although measurement-induced quantum disturbances are negligible compared to these classical contributions [59], their combined effect results in delocalized initial conditions, which in turn reduce the spreading rate of the wave function. Consequently, delocalized

states provide a more faithful representation of experimentally realizable quantum walkers, and understanding their transport behavior is essential for bridging theoretical models to practical implementations [12, 13]. In this setting, identifying conditions under which disorder, fluctuations, or lattice defects enhance spreading becomes particularly relevant, since the performance of many quantum-walk-based algorithms ultimately depends on the walker's propagation efficiency. At the same time, such mechanisms may also induce partial localization, making it necessary to assess whether the state becomes trapped near the defect.

To establish a quantitative comparison between the spreading of CTQWs on a defective lattice, governed by \hat{H}_d in Eq. (6), and on a homogeneous lattice, driven by \hat{H} in Eq. (2), we use as a figure of merit the ratio σ_d/σ between the corresponding standard deviations in the long-time regime ($\gamma t \gg 1$), following Ximenes et al. [23]. In addition, we evaluate the probability P_0 at the defect site to identify parameter regimes that lead to localization.

Figure 3 characterizes the influence of the defect parameters (ξ, θ_+) on localization in CTQWs initialized from Gaussian states with different widths. Panels (a) and (b) show the probability P_0 at the defect as a function of the hopping-amplitude ratio ξ for (a) identical defect phases ($\Delta \theta = 0$) and (b) opposite phases ($\Delta \theta = \pi$). The nonmonotonic dependence of P_0 on ξ reflects two distinct localization mechanisms. For small $|\xi|$, the defect site becomes weakly coupled to its neighbors, effectively isolating it and trapping probability, thereby suppressing transport. As $\xi \to 1$, the system recovers translational invariance and P_0 converges to the defect-free value, indicating fully delocalized dynamics. For $|\xi| > 1$, however, the defect bonds exceed the background coupling, creating a strong-bond defect that supports localized or quasi-localized modes. In this regime, a fraction of the amplitude oscillates between the defect and its nearest neighbors without propagating away, yielding a secondary increase in P_0 . This revival of localization at large $|\xi|$, arising from strong-coupling-induced reflection, is closely analogous to bound-state formation in tightbinding lattices with a local on-site impurity [60, 61].

Panels (a) and (b) of Fig. 3 also highlight a pronounced asymmetry for Gaussian initial states and a restoration of symmetry when opposite phases are applied. This behavior originates from phase-induced chirality: localized initial states, whose evolution begins solely at j=0, preserve spatial symmetry, whereas Gaussian states distribute amplitude over multiple sites and acquire different phases when propagating from $j=\pm 1$ toward the defect. These phase-shifted contributions generate a directional bias in the probability flow. When the phase difference satisfies $\Delta\theta=\pi$, destructive interference removes this bias, restoring the symmetric profile and demonstrating direct control of state localization via local phase tuning.

Figure 4 further show that the defect-site probability decays as $P_0 \propto (\gamma t)^{-1}$, vanishing in the long-time

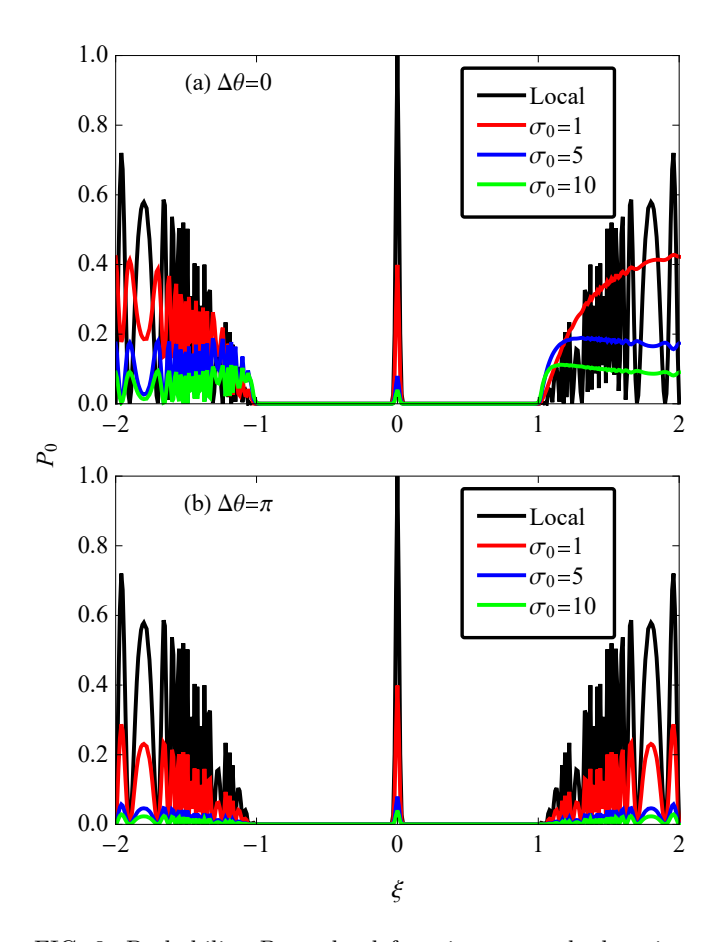


FIG. 3. Probability P_0 at the defect site versus the hopping amplitude ξ for (a) equal phases and (b) opposite phases. Panel (a) exhibits phase-induced chirality for Gaussian states, whereas opposite phases in (b) restore reflection symmetry. The fully localized state (black) is $|\psi_0\rangle = |0\rangle$, and Gaussian states have initial standard deviations $\sigma_0 = 1$ (red), 5 (blue), and 10 (green). All simulations were run to $\gamma t = 1000$.

limit. This power-law decay confirms that the defect does not support persistent trapping in this regime, consistent with the known return-probability scaling of one-dimensional CTQWs [16]. Thus, although phase defects can transiently influence state localization, they do not generate long-lived bound states under the parameters explored here.

Figure 5 illustrates how the defect parameters (ξ, θ_{\pm}) influence transport in CTQWs initialized from Gaussian states with different widths. Panels (a) and (b) further confirm the chiral effect, showing asymmetric and symmetric profiles of σ_d/σ , respectively, when the phases are equal or opposite. Together with the probability distributions, these results demonstrate direction-dependent propagation for Gaussian initial states under equal phases, consistent with earlier observations [52]. They also reveal a striking feature: while a localized state shows a modest enhancement of approximately 39% in σ_d/σ , this improvement grows markedly with σ_0 , reaching values multiple times larger for highly delocalized states. Thus, although delocalized states propagate more

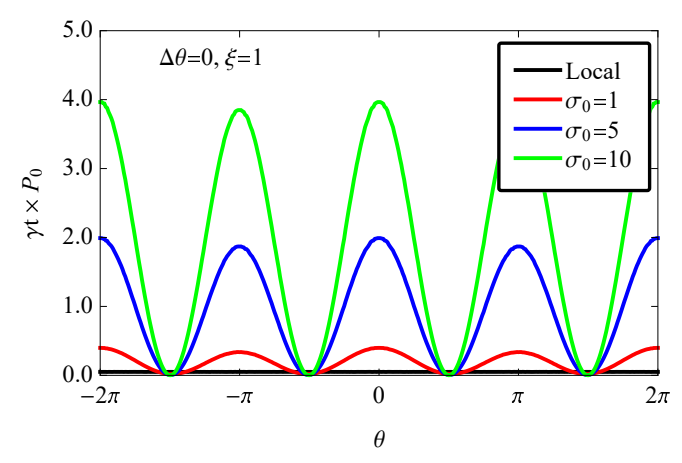


FIG. 4. Rescaled probability $\gamma t P_0$ versus θ for $\theta_{\pm} = \theta$ with $\xi = 1$. Phase effects decay as $P_0 \propto (\gamma t)^{-1}$ and vanish in the long-time limit. The fully localized case (black) is $|\psi_0\rangle = |0\rangle$, and initial Gaussian states have $\sigma_0 = 1$ (red), 5 (blue), and 10 (green). All simulations were run to $\gamma t = 1000$.

slowly on a homogeneous lattice, the presence of a single local defect can substantially boost their transport efficiency—exceeding even the gains observed for a localized walker. Moreover, an equally pronounced enhancement can be achieved via phase engineering. As shown in panels (c) and (d), when the hopping amplitude is fixed at $\xi=1$, tuning only the phases θ_{\pm} is sufficient to produce a comparable increase in the spreading rate.

Phase control in CTQWs has recently emerged as a powerful mechanism for manipulating quantum interference and steering transport. Engineered phases, combined with suitable graph structures and initial states, can selectively suppress the occupation of target sites without hindering global spreading [53, 62], and can likewise enhance propagation by coherently modulating interference pathways [22, 23]. The results in Figs. 3 and 5 demonstrate these mechanisms in a minimal setting for delocalized states: phase modulation enables or suppresses directional transport without altering the asymptotic delocalized regime, and can even enhance propagation by reshaping interference-driven spreading dynamics. This tunability underscores the role of phases as an accessible and versatile resource for coherent control in quantum walks.

Our results so far indicate that appropriate choices of (ξ,θ_\pm) can substantially enhance the transport of quantum information by Gaussian states, either symmetrically or with directional bias. Although this highlights a distinctive feature of delocalized wave packets, it also reveals parameter regimes that are unfavorable for propagation. As shown in panel (c) of Fig. 5, for $\sigma_0=1$ the ratio σ_d/σ exhibits minima at $\xi=1$ and $\theta=\pm\pi/3,\pm5\pi/3$, corresponding to conditions where $\sigma_d/\sigma<1$. These minima motivate a systematic search for poorer-spreading configurations, which then serve as the individual "losing" strategies underpinning the Parrondo-type alterna-

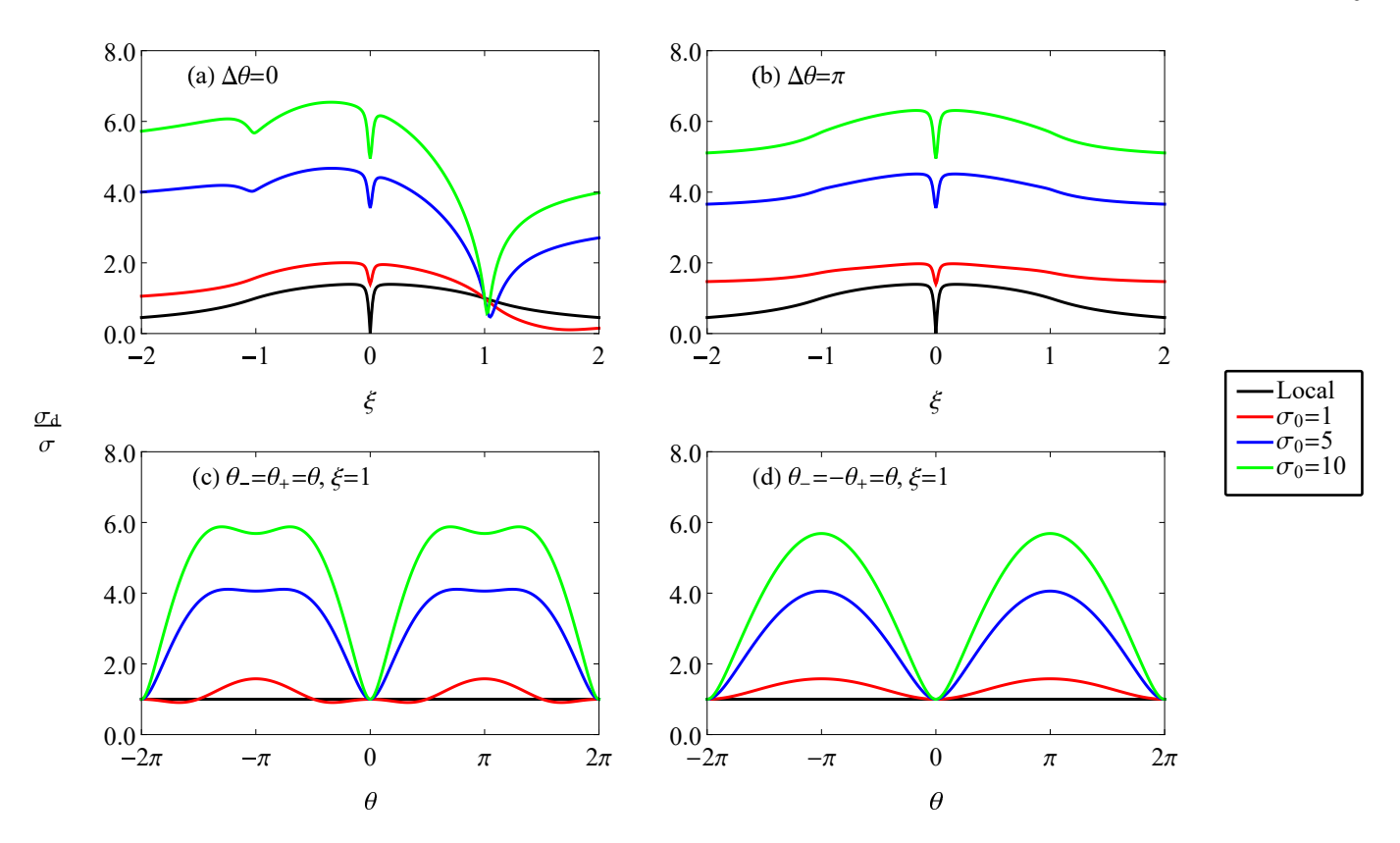


FIG. 5. Ratio σ_d/σ between the standard deviations in the defective and homogeneous lattices, plotted versus ξ for (a) equal phases and (b) opposite phases, and versus θ for (c) $\theta_- = \theta_+ = \theta$ and (d) $\theta_- = -\theta_+ = \theta$, with $\xi = 1$ in (c,d). Equal phases in (a) lead to asymmetric spreading for Gaussian states, whereas opposite phases in (b) eliminate this asymmetry. Gaussian states exhibit a stronger response to the defect than the fully localized state. The localized state (black) corresponds to $|\psi_0\rangle = |0\rangle$, and initial Gaussian states have $\sigma_0 = 1$ (red), 5 (blue), and 10 (green). All simulations were run to $\gamma t = 1000$.

tion protocol for a Gaussian state examined in the next section.

C. Parrondo protocol with a Gaussian state

Parrondo's effect, originally introduced in game theory, describes situations in which individually losing strategies, when alternated, yield an overall winning outcome [26, 27]. In the present setting, a losing strategy corresponds to a CTQW on a defective lattice whose parameters (ξ, θ_{\pm}) produce a spreading rate lower than that of the homogeneous case. Ximenes et al. investigated this phenomenon for localized initial states by alternating between two real-valued defect parameters [23]. Because delocalized states on defective lattices typically outperform the homogeneous lattice, it is first necessary to identify regions of parameter space where their spreading is reduced, so that losing strategies can be appropriately defined.

Figure 6 shows a contour map of the ratio σ_d/σ as a function of the defect parameters (ξ, θ) for the configuration $\theta_- = -\theta_+ = \theta$, whose behavior closely resembles the case $\theta_- = \theta_+ = \theta$. The color scale makes clear that the spreading efficiency depends sensitively

on both the hopping-amplitude ratio ξ and the phase θ . Near the homogeneous limit ($\xi \approx 1, \theta \approx 0$), the contour map displays a narrow band of values close to unity (light-green region), consistent with $\sigma_d/\sigma \simeq 1$. In contrast, two extended regions of suppressed spreading appear as dark-blue lobes centered around the parameters $(\xi \simeq 2, \theta \simeq 0, 2\pi)$ and $(\xi \simeq -2, \theta \simeq \pm \pi)$, where $\sigma_d/\sigma < 1$. These minima arise from strong-bond defects that generate reflection-dominated dynamics: constructive interference between left- and right-moving components traps a significant fraction of the probability density near the defect, thereby inhibiting global spreading. By comparison, a broad yellow-orange region emerges for $-1 < \xi < 1$ over the full range of θ , indicating $\sigma_d/\sigma > 1$ and therefore enhanced spreading. This enhancement arises from destructive interference between left- and right-moving components induced by the reduced defect coupling, which biases transport away from the defect, although a considerable fraction of probability remains weakly trapped. The smooth color transitions surrounding the enhancement and suppression zones show how the boundaries between these regimes shift continuously as ξ departs from unity, demonstrating that local hoppingamplitude imbalance, together with phase modulation, jointly shapes the transport behavior.

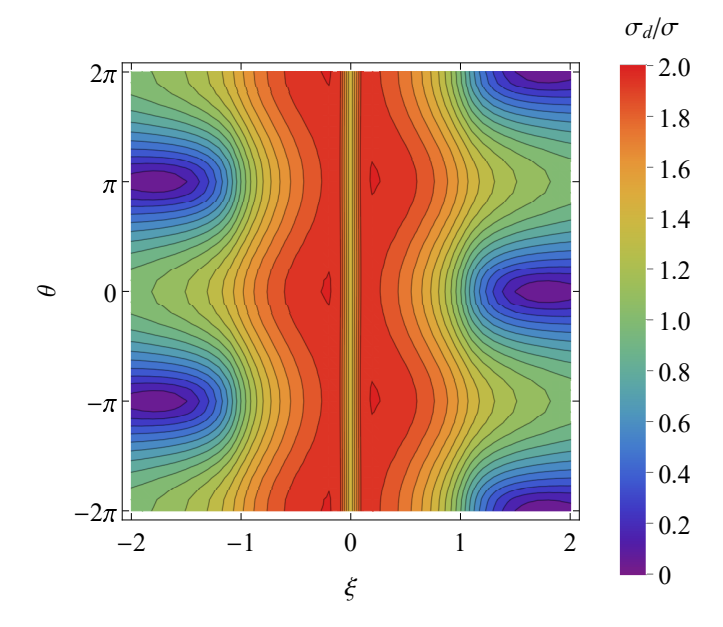


FIG. 6. Contour plot of the ratio σ_d/σ as a function of the defect parameters ξ and θ . The simulation was performed for a Gaussian initial state ($\sigma_0 = 1$) and evolved up to $\gamma t = 1000$.

After extensive testing, we selected the losing strategies A, B, C, and D listed in Table I. These strategies define the three Parrondo alternation protocols AB, CB, and CD investigated here. As discussed earlier, each protocol evolves the state in time intervals of π/ω , switching between two distinct losing strategies at successive steps. For each protocol, we analyze the dependence on ω to identify the optimal value that maximizes the spreading enhancement as shown in Fig. 7.

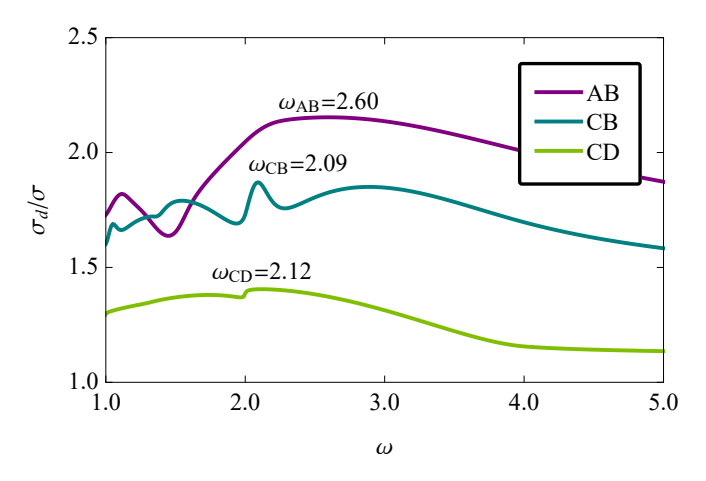


FIG. 7. Ratio σ_d/σ as a function of the parameter ω . The value of ω selected for each alternation protocol is indicated in the figure. Simulations were performed for a Gaussian initial state ($\sigma_0 = 1$) and evolved up to $\gamma t = 2000$.

Figure 8 displays the transport features of the four losing strategies, which capture distinct dynamical behaviors of CTQWs on defective lattices, together with

the outcomes of the three Parrondo alternation protocols constructed from them. Panels (a)-(c) display the probability distributions P(j) for the individual losing strategies. Panel (a) shows that both strategies A and B produce nearly symmetric profiles with pronounced localization around the defect site. Strategy A exhibits strong trapping, concentrating approximately 97% of the total probability for $j \in [-4, 4]$, whereas B retains about 76% in the same interval, as shown in the inset. Although their global spreading differs, both cases display severely hindered transport. The case B highlights the importance of jointly examining spreading and localization: its standard deviation is only about 9% smaller than that of the homogeneous lattice, yet the walker's transport remains substantially inhibited. More generally, a defect configuration may satisfy $\sigma_d/\sigma > 1$ while still exhibiting noticeable local trapping, showing that enhanced spreading does not imply the absence of localization. The remaining losing strategies, C and D, shown in panels (b) and (c), generate asymmetric (left- and right-biased) distributions with only weak residual localization near the defect. Even in the absence of strong trapping, these strategies still fail to achieve efficient spreading, demonstrating that poor transport does not require pronounced localization.

Panels (d)–(f) present the probability distributions obtained from alternating the corresponding losing strategies in time. In all three cases, the alternation protocol eliminates the localization present in the individual strategies, yielding broad distributions that exceed the homogeneous benchmark H (black dashed). The suppression of trapping arises because each half-evolution step disrupts the constructive interference responsible for localization in the individual strategies, allowing probability to escape from the defect region: the state is effectively "pushed away" from the defect, eliminating trapping and promoting outward transport. Beyond merely removing localization, the alternation generates a qualitatively new dynamical regime, which converts two individually poor-spreading evolutions into a markedly enhanced one.

The consequences of this enhancement are quantified in panels (g)–(i), which show the time dependence of the standard deviation $\sigma(t)$ for each pair of losing strategies and for their alternated evolution. In every case, the alternation protocol produces a significantly larger $\sigma(t)$ than either of its constituent losing strategies and even surpasses the homogeneous evolution for long times. The

TABLE I. Defect parameters for each losing strategy (LS) and the corresponding spreading ratio σ_d/σ at $\gamma t = 1000$.

$\begin{array}{cccccccccccccccccccccccccccccccccccc$	0.36
B $1.4 -3/2 3/2$	
	0.91
C -1.0 $11/10$ $11/1$	0.98
D -1.0 9/10 9/10	0.98

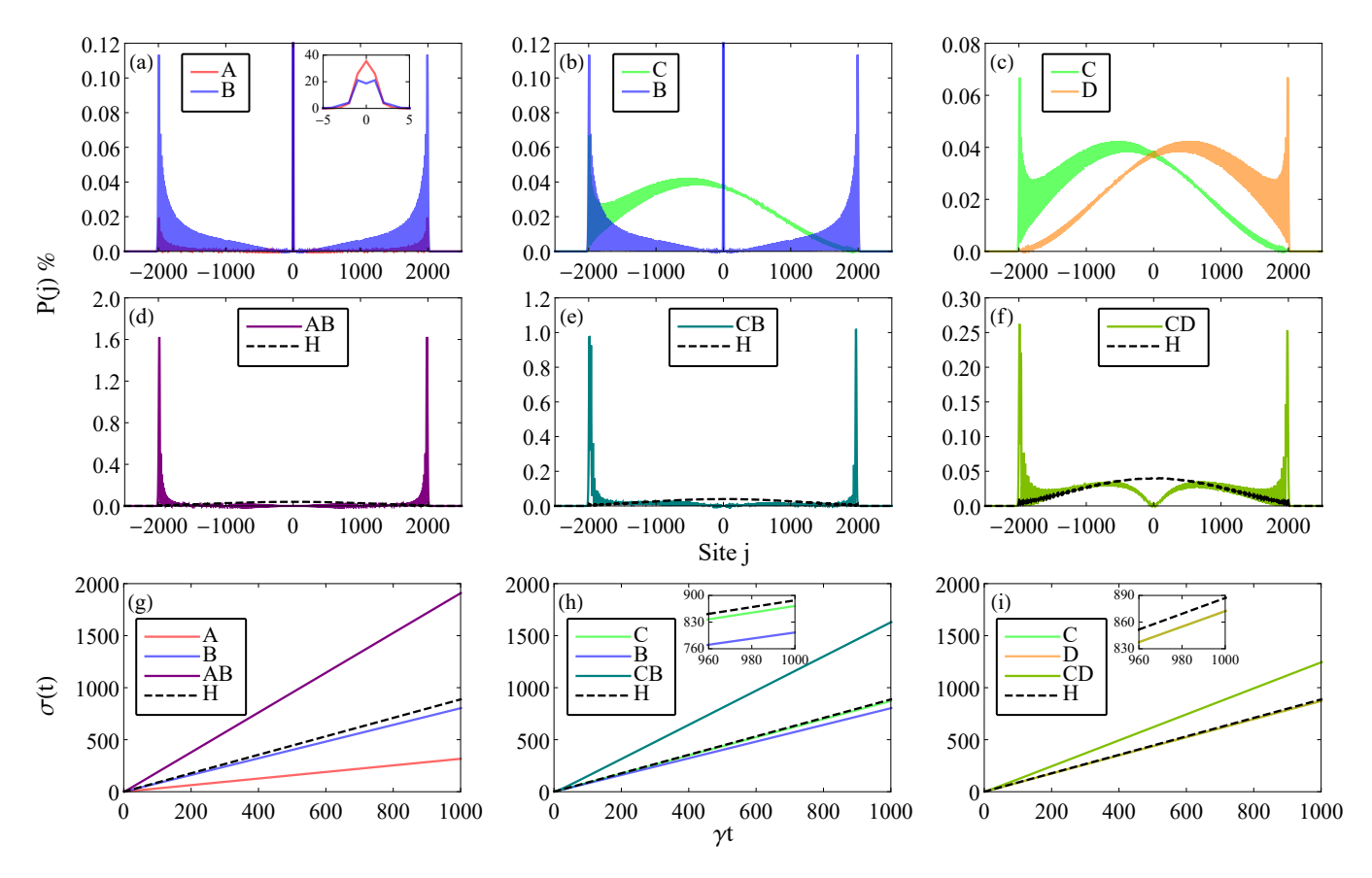


FIG. 8. Probability distribution P(j) for the losing strategies A (red), B (blue), C (green), and D (orange) in panels (a)–(c), and for the alternation protocols AB (purple), CB (dark teal), and CD (lime green) in panels (d)–(f). Panels (g)–(i) show the corresponding standard deviation $\sigma(t)$ as a function of time, comparing each pair of losing strategies with its respective Parrondo alternation protocol. The strategies are defined by the defect parameters A: $(\xi = -1.8, \theta_- = -1.2\pi, \theta_+ = 1.2\pi)$, B: $(\xi = 1.4, \theta_- = -1.5\pi, \theta_+ = 1.5\pi)$, C: $(\xi = -1.0, \theta_\pm = 1.1\pi)$, and D: $(\xi = -1.0, \theta_\pm = 0.9\pi)$. The homogeneous lattice H (black dashed) is included for reference. The insets in panels (h) and (i) show that C, B, and D remain below H throughout the evolution; in panel (i), the curves for C and D are nearly indistinguishable. All simulations were performed for a Gaussian initial state with $\sigma_0 = 1$ and evolved up to $\gamma t = 1000$.

insets in panels (h) and (i) confirm that the individual strategies B, C, and D remain below the homogeneous curve throughout the evolution, emphasizing that each strategy is indeed "losing." In contrast, the alternated sequence displays sustained growth with an asymptotic slope larger than that of all individual evolutions. The nearly overlapping curves for C and D in panel (i) further illustrate the robustness of this behavior for strategies with similar dynamical signatures.

Taken together, the results in Fig. 8 demonstrate that alternating two losing strategies can suppress defect-induced localization, restore long-range transport either symmetrically [panels (d) and (f)] or with directional bias [panel (e)], and produce a spreading rate that exceeds both individual dynamics and the homogeneous quantum walk. This constitutes a clear realization of a Parrondo-type effect for CTQWs initialized from Gaussian states.

IV. CONCLUDING REMARKS

We studied the transport properties of continuous-time quantum walks (CTQWs) initialized in delocalized states on a one-dimensional lattice with a single defect. The defect is implemented through a modified hopping amplitude ξ and complex phases θ_- and θ_+ applied to the left and right bonds connecting the walker's central site to its nearest neighbors. We focused on the contrasting behaviors that arise when the walker is initialized either in a fully localized state or in Gaussian states of different widths. Like localized states, Gaussian wave packets are sensitive to the defect strength, but they additionally display a phase-induced chirality absent in the localized case. We further showed that their dynamics reflect a competition between weak- and strong-coupling localization mechanisms, each modulated by the applied phases.

Our results show that suitable choices of (ξ, θ_{\pm}) can significantly enhance transport for Gaussian initial states, even though delocalization typically slows spread-

ing on homogeneous lattices. In particular, phase engineering enables fine control over directional propagation, allows suppression or restoration of spatial symmetry, and can boost the asymptotic spreading rate without inducing persistent localization. Conversely, we identified broad regions of parameter space where the standard deviation is reduced, or where noticeable trapping persists despite $\sigma_d/\sigma>1$, demonstrating that spreading efficiency and localization must be examined jointly when characterizing transport.

Mapping the (ξ,θ) parameter space revealed extended regions of enhanced and suppressed spreading governed by the interplay between hopping-amplitude imbalance and phase modulation. Regions of poor transport, identified through $\sigma_d/\sigma < 1$ for $\sigma_0 = 1$, provided the foundation for defining losing strategies in a Parrondo-type framework. Using these configurations, we constructed three alternation protocols, each formed by switching between two individually losing strategies at time intervals of π/ω . For appropriately chosen ω , the alternation protocols suppress localization, redistribute trapped probability, and achieve spreading rates that surpass those of both constituent strategies and the homogeneous lattice. This behavior underscores how temporal alternation between static defects can generate constructive interfer-

ence patterns that enhance global transport.

Overall, our findings demonstrate that defect engineering, phase control, and temporal alternation protocols constitute accessible resources for manipulating quantum states in CTQWs and improving their transport properties. The interplay of these mechanisms offers new avenues for steering quantum transport, designing quantum-walk-based algorithms, and developing controllable quantum network architectures. Extensions to multi-defect systems, higher-dimensional geometries, and explicitly time-dependent control protocols provide natural directions for future work.

ACKNOWLEDGMENTS

This work was supported by Conselho Nacional de Desenvolvimento Científico e Tecnológico (CNPq) through grant number 409673/2022-6 and by the National Institute for Science and Technology of Quantum Information (INCT-IQ) under Grant number 465469/2014-0. Computational resources were provided by the Centro Nacional de Processamento de Alto Desempenho em São Paulo (CENAPAD-SP). E. P. M. Amorim thanks J. Longo for her careful reading of the manuscript.

- Y. Aharonov, L. Davidovich, and N. Zagury, Phys. Rev. A 48, 1687 (1993).
- E. Farhi and S. Gutmann, Phys. Rev. A 58, 915 (1998).
- [3] J. Kempe, Contemp. Phys. 44, 307 (2003).
- [4] S. E. Venegas-Andraca, Quantum Inf. Process. 11, 1015 (2012).
- [5] N. Shenvi, J. Kempe, and K. Birgitta Whaley, Phys. Rev. A 67, 052307 (2003).
- [6] A. Tulsi, Phys. Rev. A 78, 012310 (2008).
- [7] R. Portugal, Quantum Walks and Search Algorithms (Springer, Cham, 2013).
- [8] G. S. Engel, T. Calhoun, E. L. Read, T.-K. Ahn, T. Mančal, Y.-C. Cheng, R. E. Blankenship, and G. R. Fleming, Nature 446, 782, (2007).
- [9] M. Mohseni, P. Rebentrost, S. Lloyd, and A. Aspuru-Guzik, J. Chem. Phys. 129, 174106 (2008).
- [10] A. M. Childs, Phys. Rev. Lett. 102, 180501 (2009).
- [11] N. B. Lovett, S. Cooper, M. Everitt, M. Trevers, and V. Kendon, Phys. Rev. A 81, 042330 (2010).
- [12] J. Wang and K. Manouchehri, *Physical implementation* of quantum walks (Springer, Heidelberg, 2013).
- [13] F. Flamini, N. Spagnolo, and F. Sciarrino, Rep. Prog. Phys. 82, 016001 (2019).
- [14] R. Vieira, E. P. M. Amorim, and G. Rigolin, Phys. Rev. Lett. 111, 180503, (2013).
- [15] R. Vieira, E. P. M. Amorim, and G. Rigolin, Phys. Rev. A 89, 042307, (2014).
- [16] N. Konno, Quantum Inf. Process. 9, 405 (2010).
- [17] A. Wójcik, T. Łuczak, P. Kurzynski, A. Grudka, T. Gdala, and M. Bednarska-Bzdega, Phys. Rev. A 85, 012329 (2012).

- [18] Z. J. Li, J. A. Izaac, and J. B. Wang, Phys. Rev. A, 87, 012314 (2013).
- [19] R. Zhang, P. Xue, and J. Twamley, Phys. Rev. A 89, 042317 (2014).
- [20] T. Endo, N. Konno, E. Segawa, and M. Takei, Yokohama Math. J. 60, 49 (2014).
- [21] L. I. da S. Teles and E. P. M. Amorim, Braz. J. Phys. 51, 911 (2021).
- [22] Z. J. Li and J. B. Wang, Sci. Rep. 5, 13585 (2015).
- [23] J. J. Ximenes, M. A. Pires, and J. M. Villas-Bôas, Phys. Rev. A 109, 032417 (2024).
- [24] J. P. Keating, N. Linden, J. C. F. Matthews, and A. Winter, Phys. Rev. A 76, 012315 (2007).
- [25] J. W. Lai and K. H. Cheong, Nonlinear Dyn. 100, 849 (2020).
- [26] G. P. Harmer and D. Abbott, Fluctuation and Noise Letters, 2, R71-R107 (2002).
- [27] J. J. Shu and Q. W. Wang, Sci. Rep. 4, 4244 (2014).
- [28] J.-P. Capp, A. M. Nedelcu, A. M. Dujon, B. Roche, F. Catania, B. Ujvari, C. Alix-Panabières, and F. Thomas, Cancers 13, 2197 (2021).
- [29] K. H. Cheong, J. M. Koh, and M. C. Jones, ByoEssays 41, 1900027 (2019).
- [30] C. S. Gokhale, and N. Sharma, R. Soc. Open Sci. 10, 221401 (2023).
- [31] Y. Ye, K. H. Cheong, Y.-W. Cen, and N.-G. Xie, Sci. Rep. 6, 37028 (2016).
- [32] A. Mishra, T. Wen, and K. H. Cheong, Phys. Rev. Research 6, L012037(2024).
- [33] C. M. Chandrashekar and S. Banerjee, Phys. Lett. A **375**, 1553 (2011).
- [34] A. P. Flitney, arXiv:1209.2252.

- [35] M. Li, Y. S. Zhang, and G. C. Guo, Fluctuation and Noise Lett. 12, 1350024 (2013).
- [36] J. Rajendran and C. Benjamin, R. Soc. Open Sci. 5, 171599 (2018).
- [37] J. W. Lai, J. R. A. Tan, H. Lu, Z. R. Yap, and K. H. Cheong, Phys. Rev. E 102, 012213. (2020).
- [38] M. A. Pires and S. M. D. Queirós, Phys. Rev. E 102, 042124 (2020).
- [39] M. Jan, Q. Q. Wang, X. Y. Xu, W. W. Pan, Z. Chen, Y. J. Han, and D. Abbott, Adv. Quantum Technol. 3, 1900127 (2020).
- [40] D. K. Panda, B. V. Govind, and C. Benjamin, Physica A 608, 128256 (2022).
- [41] G. Trautmann, C. Groiseau, and S. Wimberger, Fluctuation and Noise Lett. 21, 2250053 (2022).
- [42] B. Tregenna, W. Flanagan, R. Maile, and V. Kendon, New J. of Phys. 5, 83 (2003).
- [43] G. J. de Valcárcel, E. Roldán, and A. Romanelli, New J. of Phys. 12, 123022 (2010).
- [44] A. Romanelli, Phys. Rev. A 81, 062349 (2010).
- [45] W.-W. Zhang, S. K. Goyal, F. Gao, B. C. Sanders, and C. Simon, New J. of Phys. 18, 093025 (2016).
- [46] A. C. Orthey and E. P. M. Amorim, Quantum Inf. Process. 16, 224 (2017).
- [47] A. C. Orthey and E. P. M. Amorim, Phys. Rev. A 99, 032320 (2019).
- [48] A.C. Orthey and E. P. M. Amorim, Braz. J. Phys. 49, 595 (2019).
- [49] H. S. Ghizoni and E. P. M. Amorim, Braz. J. Phys. 49, 168 (2019).

- [50] R. Vieira, G. Rigolin, and E. P. M. Amorim, Phys. Rev. A 104, 032224 (2021).
- [51] J. P. Engster, R. Vieira, E. I. Duzzioni, and E. P. M. Amorim, Quantum Inf. Process. 23, 103 (2024).
- [52] A. Khalique, A. Sett, J. B. Wang, and J. Twamley, New J. Phys. 23, 083005 (2021).
- [53] R. Chaves, B. Chagas, and G. Coutinho, Quantum Inf. Process. 22, 41 (2023).
- [54] A. Bottarelli, M. Frigerio, and M. G. Paris, AVS Quantum Sci. 5, 025001 (2023).
- [55] T. G. Wong, L. Tarrataca, and N. Nahimov, Quantum Inf. Process. 15, 4029 (2016).
- [56] C. Cohen-Tannoudji, B. Diu, and F. Laloë, Quantum Mechanics (Wiley-VCH, Weinheim, 2020).
- [57] N. Zettili, Quantum Mechanics: concepts and applications (John Wiley & Sons, Chichester, 2009).
- [58] D. H. McIntyre, Quantum Mechanics: a paradigms approach (Pearson Education, San Francisco, 2012).
- [59] A. Peres, Quantum theory: concepts and methods (Kluwer Academic Publishers, 2002).
- [60] N. W. Ashcroft and N. D. Mermin, Solid State Physics (Holt, Rinehart and Winston, New York, 1976).
- [61] C. Kittel, Introduction to Solid State Physics, 8th ed. (Wiley, Hoboken, NJ, 2005).
- [62] A. Sett, H. Pan, P. E. Falloon, and J. B. Wang, Quantum Inf. Process. 18, 159 (2019).